Environ. Water Eng., 2025, 11(1), 37-46 DOI: 10.22034/ewe.2024.455792.1930

EWE

Environment and Water Engineering

Homepage: www.jewe.ir

ISSN: 2476-3683

Evaluation of subsidence phenomenon by Multilayer Perceptron Artificial Neural Network (Case Study: Dehgolan Plain, Kurdistan Province, Iran)

Seyed Mohammad Hosseini[1], Mohsen Isari[1]✉, Jamil Bahrami[1], Sajjad Karimi[2], and Farhad Faghihi[3]

[1]Department of Civil Engineering, Faculty of Engineering, University of Kurdistan, Sanandaj, Kurdistan, Iran
[2]Department of Mapping Engineering, Faculty of Engineering, Khajeh Nasiruddin Tosi University, Tehran, Iran
[3]Department of Surveying Engineering, Technical and Vocational University, Tehran, Iran

ARTICLE INFO

Paper Type: Research Paper

Received: 07 May 2024
Revised: 09 July 2024
Accepted: 04 August 2024
Published: 21 March 2025

Keywords
Multilayer perceptron
Groundwater levels
Alluvial thickness
Land subsidence

Corresponding author:
M. Isari
✉ m.isari@uok.ac.ir

ABSTRACT

Subsidence poses a significant management challenge, causing damage to infrastructure, energy transmission lines, buildings, soil stability, and leading to the formation of sinkholes. This study employed the Multilayer Perceptron (MLP) neural network to evaluate and model the extent of subsidence in the Dehgolan Plain aquifer, located in Kordestan Province, between March 23, 2022, and September 24, 2023. A subsidence model was constructed using groundwater level data, changes in transmissivity, alluvial thickness, and results from radar interferometry. Regression analysis comparing predicted and observed values confirmed the model's high accuracy in forecasting subsidence. Furthermore, the model successfully estimated missing subsidence rates. The maximum subsidence calculated using radar interferometry over the 552-day period was 154 mm, while the maximum uplift was 16 mm. In comparison, the MLP model estimated a maximum subsidence of 145 mm and a maximum uplift of 12 mm. Subsidence was found to be more pronounced in the western and central regions of the plain compared to the eastern areas. Considering the ongoing progression of subsidence in the Dehgolan Plain aquifer, it is imperative to implement strategies to reduce the over-extraction of groundwater and establish continuous monitoring systems.

How to cite this paper:
Isari, M., Hosseini, S. M., Faghihi, F., Bahrami, J., & Karimi, S. (2025). Evaluation of subsidence phenomenon by Multilayer Perceptron Artificial Neural Network (case study: Dehgolan Plain, Kurdistan Province). *Environ. Water Eng.*, *11*(1), 37-.46. doi: 10.22034/ewe.2024.455792.1930

1. Introduction

Land subsidence is a significant management hazard, resulting in damages to infrastructure, gas and power transmission lines, buildings, the formation of sinkholes, coastal flooding, and soil degradation (Ranjgar et al., 2021). Excessive groundwater extraction increases the effective stress within aquifers, altering the density of fine-grained sediment particles and leading to land subsidence in affected regions. The extensive areas prone to or experiencing subsidence present challenges in terms of monitoring costs. Installing on-site monitoring equipment and deploying new satellites are expensive, prompting greater reliance on remote sensing techniques (Edalat et al., 2020). Remote sensing provides high accuracy, comparable to leveling measurements and global positioning systems, even at millimeter scales.

Neural networks have emerged as an effective tool for addressing modern challenges. These networks excel at identifying general, low-precision relationships within data and applying them to real-world analysis. Additionally, neural networks can recognize patterns and relationships between variables and predict missing data after adequate training (Banerjee et al., 2011).

Globally, numerous studies have explored the application of neural networks to land subsidence. For instance, Ali et al. (2020) investigated subsidence in Taiwan, while Wang et al. (2021) studied this phenomenon in Anhui, China. Shimosato

and Ukita (2021) utilized leveling, global navigation satellite systems (GNSS), and interferometric synthetic aperture radar (InSAR) analysis to examine subsidence across 33 regions in Japan. While each method has limitations, Sato et al. employed neighborhood relationships within a convolutional neural network (CNN), reducing the mean error from 10.3 mm to 6.8 mm compared to conventional methods.

Despite their effectiveness, neural network models have limitations, including dependence on historical data. To address these shortcomings, Zhou et al. (2022) used the K-means clustering algorithm to predict land subsidence in Kunming City, Yunnan Province, China. Their study estimated a maximum subsidence rate of 30.591 mm/year between 2018 and 2021.

In Taiwan, Ku and Liu (2023) developed an artificial neural network model to analyze the relationship between electricity consumption and land subsidence in Yunlin County. A 10% reduction in electricity consumption decreased the severely subsiding area by 10%. Notably, reducing electricity consumption from 80% to 70% resulted in a 13.66% reduction in the subsidence rate.

Zhu et al. (2023) introduced a novel SSA-BP model to simulate land subsidence in Beijing's Tongzhou District. Using PS-InSAR remote sensing technology, they found that the average annual subsidence rate ranged from -133.9 mm/year to +3.9 mm/year between November 2010 and January 2020.

In a study, a novel approach was employed to enhance the classification performance of a decision tree by combining it with four machine learning algorithms to create a land subsidence susceptibility map in the central Iranian plain. A comparison of the results from various models demonstrated that the new hybrid DSC-ADTree algorithm achieved the highest accuracy of 0.983 in generating the LSSSM, outperforming other learning models (Zhao et al., 2024).

Extensive research has explored land subsidence caused by coal mining (MLS) through the application of an intelligent hybrid model integrating gradient boosting with a classified feature support algorithm. Five hybrid models based on CatBoost were developed, allowing for the comparison and analysis of their prediction accuracy and reliability. The study reported a high regression coefficient of 92.5% and a mean error of 0.52, highlighting the model's robustness and precision. These findings confirm the reliability of hybrid modeling technology as an effective approach for predicting MLS (Zhang et al., 2024).

In Iran, several studies have examined subsidence phenomena using machine learning and remote sensing methods. For instance, Radman and Akhoondzadeh (2022) combined InSAR time series data with machine learning to predict land subsidence around Lake Urmia, highlighting the influence of seasonal changes. Similarly, Asghari Moghaddam et al. (2023) applied the ALPRIF method to create a subsidence zoning map for East Azerbaijan's Ajabshir Plain, revealing a subsidence rate of 2.4 cm between 2020 and 2021.

Hosseinzadeh et al. (2024) evaluated subsidence in Iran's Semnan and Kashmar plains using a neural network model with geological and hydrological variables. The BRT model achieved accuracies of 75% and 74% in the two case studies, respectively, while the MLR method yielded mean squared errors (MSE) of 0.25 and 0.32.

The Dehgolan Plain in Kordestan Province, an important agricultural hub, has faced increased water demands due to reverse migration over the past two decades. Excessive and unsustainable groundwater use has raised concerns among policymakers and academics about subsidence risks in the region (Ahmadi and Soudmand Afshar, 2020). This study aims to develop a robust model using the Multilayer Perceptron (MLP) neural network to identify areas susceptible to subsidence over an 18-month period, from March 23, 2022, to September 24, 2023. The model incorporates geological, hydrological, and hydraulic data, alongside previous subsidence measurements, to provide a comprehensive assessment.

2. Materials and Methods

2.1. Study Area

The Dehgolan Plain, located in Kurdistan Province, Iran, lies between longitudes 47°10′ and 47°45′ East and latitudes 35°05′ and 35°35′ North. The area of the plain covers 982.42 km². The Dehgolan Plain aquifer system is situated within the coordinates of longitudes 47°11′ and 47°42′ East, and latitudes 35°06′ and 35°23′ North. The aquifer and watershed areas are 779.81 km² and 2550 km², respectively(Fig.1). The average elevation of the plain is 1876 meters above sea level. The Ibrahim Attar, Bikhir, Sarmeh Ali, Abdolrahman Ovis, Darband, and Kiwarkor mountains, located along the southwest to southeast boundaries of the study area, are among the region's prominent peaks.

2.2. Modeling of subsidence using multilayer perceptron neural networks

Among the various types of artificial neural networks used for prediction, hydrologists recommend the Multilayer Perceptron (MLP) model as the most suitable and widely used approach for hydrological modeling and assessment (Abrahart and White, 2001). Therefore, monitoring and predicting risks using this model is crucial for scientists and decision-makers.

As illustrated in Fig. 2, the Multilayer Perceptron neural network, by utilizing input and output data, can learn the relationships between inputs and outputs, enabling it to provide accurate and novel outputs based on new input data. In this study, changes in groundwater levels, aquifer transmissivity, and sediment thickness were selected as input data, while subsidence results obtained through the InSAR method were used as output data.

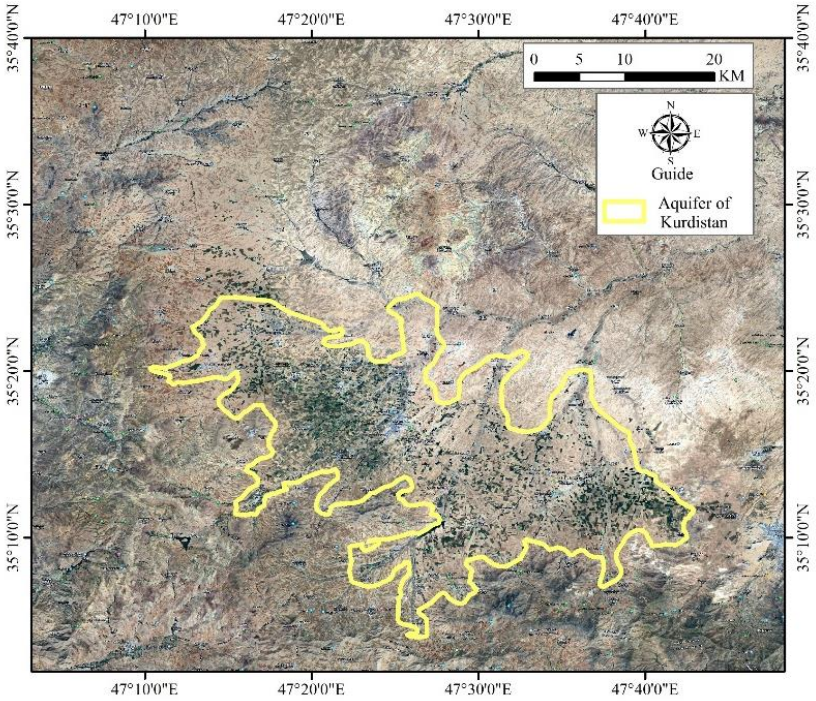

Fig. 1 Dehgolan plain aquifer

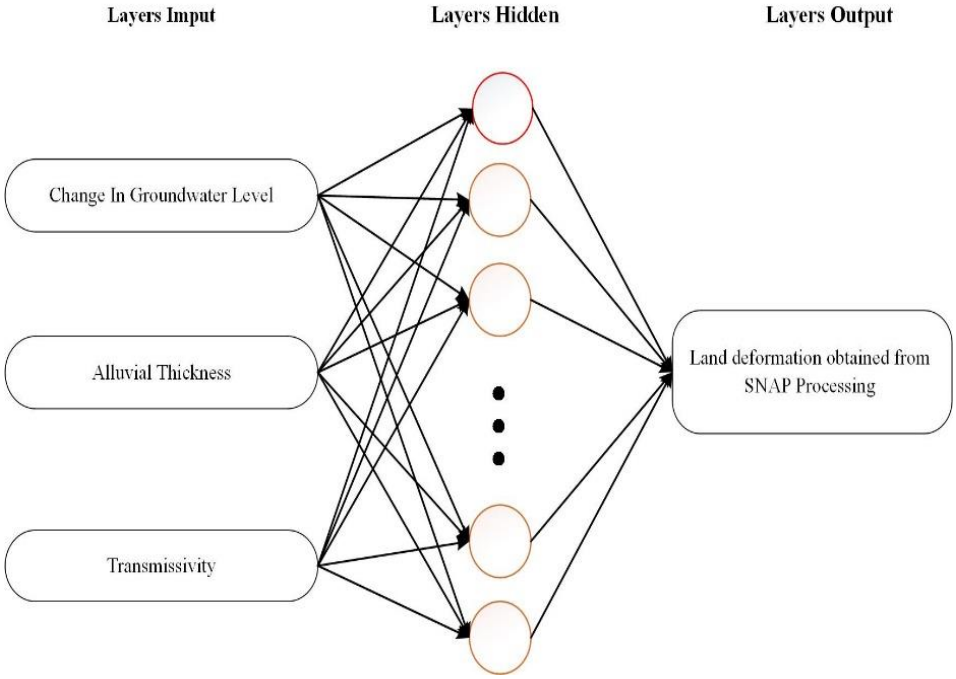

Fig. 2 Flowchart of the general architecture of the Multilayer Perceptron neural network used to calculate and model land subsidence in the Dehgolan Plain.

2.3. Data utilized in the multilayer perceptron neural network

2.3.1. Input data for the MLP neural network

Using data from 107 observation wells and 16 exploratory wells, the groundwater level in the Ghorveh and Dehgolan plain was estimated to range from 1740 m to 1940 m. Based on field test results and observations, groundwater level ratios over time were analyzed, and spatial graphs were plotted to identify areas with similar geometric attributes for groundwater level, sediment thickness, and aquifer transmissivity (Fig. 3). Analysis of the groundwater level data reveals a general trend of decreasing levels from the west and northwest towards the central part of the plain. Conversely, an increase in groundwater levels is observed from the central region towards the southeastern and occasionally southern areas of the plain. The lowest groundwater level, measured at 1740 m, occurs in the Saeidabad village and Dehgolan city areas in the plain's central region. In contrast, the highest groundwater level, at 1940 m, was observed at the

westernmost points of the plain, particularly in the lands of Ibrahim Abad, Kani Pahn, and portions of Haji Pamq village (Anonymous, 2018). As shown in Fig. 3, the trend of groundwater level and rainfall changes from 1366 to 1401 in the Dehgolan plain aquifer of Kurdistan Province demonstrates a downward trajectory. This indicates a significant decline in annual rainfall over the years. Furthermore, increased groundwater extraction has exacerbated the reduction in groundwater levels in recent years within this region.

Based on the findings from field tests and observation wells, the thickness of resistant alluvial deposits varies across different regions of the study area, ranging from a maximum of 120 m to a minimum of 20 m. The greatest alluvial thickness is observed in the central part of the plain and near urban areas (Anonymous, 2018).

According to the results of pumping tests conducted in exploratory wells, a zoning map was created. Analysis of the results indicates that, in general, moving from the highlands towards the center of the aquifer and the plain, the thickness and depth of the aquifer increase while the transmissivity decreases. However, as the coarseness and heterogeneity of the layers increase, the transmissivity also rises. In the Dehgolan Plain study area, the aquifer transmissivity ranges from 144 to 1492 m²/day. The highest values are observed in the villages of Haji Pemaq and Mubarak Abad Koleresh, while the lowest values are located in the eastern and central parts of the plain (Anonymous, 2018).

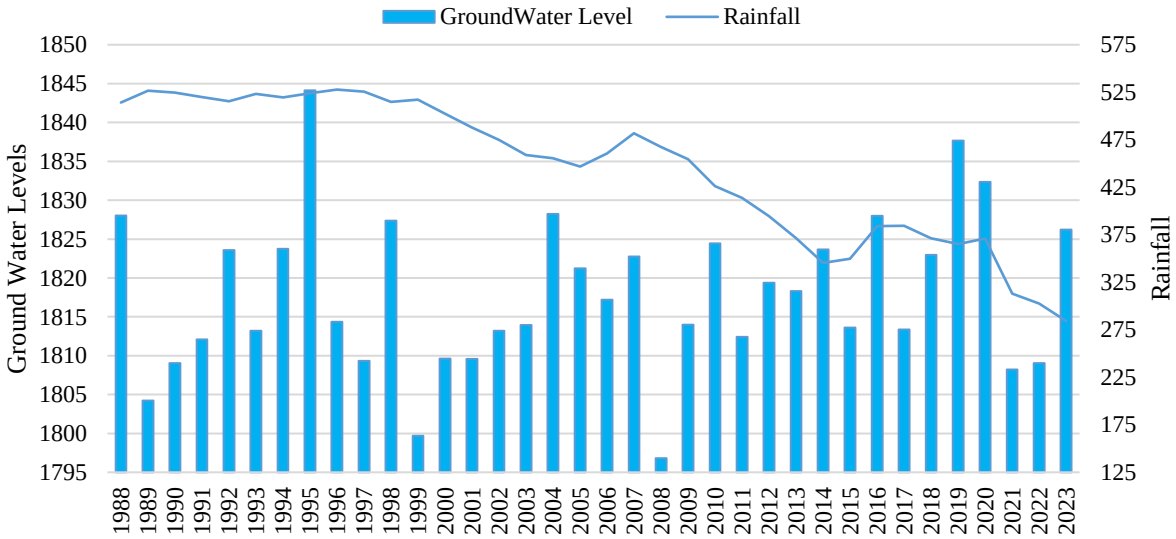

Fig. 3 The graph illustrating changes in groundwater levels and rainfall within the Dehgolan Plain aquifer during the statistical period from 1987–1988 to 2022–2023

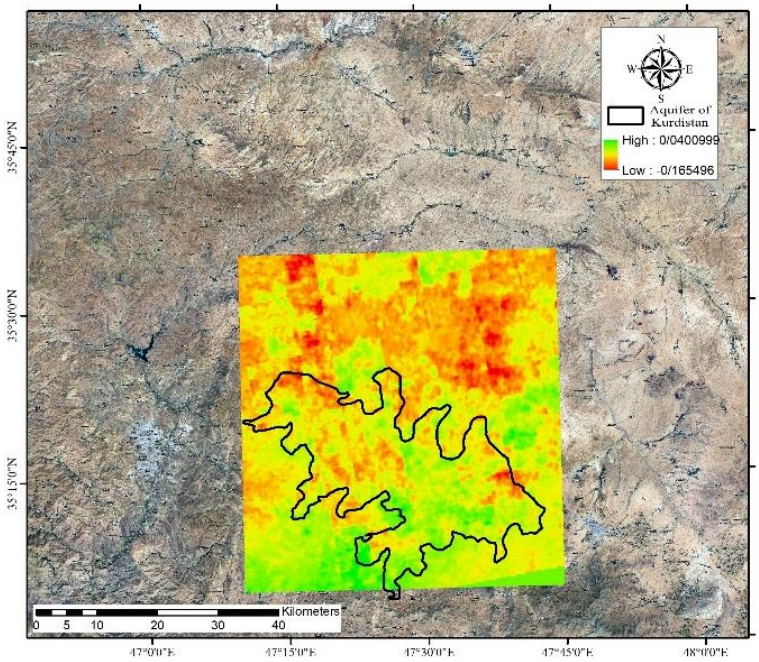

Fig. 4 Displacements Obtained from Sentinel-1 Satellite Images in Dehgolan Plain of Kurdistan Province during Time Interval t_1

2.3.2. Output information of the MLP neural network

Vertical displacement and crustal changes, including subsidence and uplift, over a specific time period in the Dehgolan Plain, were analyzed using Sentinel-1 satellite imagery and SNAP software. The results derived from the output data were utilized to monitor and develop a subsidence model using a multilayer perceptron (MLP) neural network. According to radar interferometry results (Fig. 4), the maximum vertical crustal displacement in the form of subsidence over a 552-day period in the Dehgolan Plain of Kurdistan Province is -165.4 mm, while the maximum vertical displacement in the form of uplift is +41 mm.

To evaluate the model's performance, subsidence values calculated at shorter time intervals within the 552-day period were also employed (Table 1). Some pixels are displayed in black due to the absence of phase displacement values, represented as zero or NaN in the matrix. Additionally, to enhance generalizability, subsidence data over shorter time intervals were incorporated. Specifically, the subsidence results computed via interferometry over 96 and 60 days (between t_6 and t_7, and t_1, respectively) were utilized for model training and prediction.

Table 1 Specifications of Time Periods Used for Subsidence Analysis and Modeling

Time	Duration	Start Date	Ending Date
t_1	552	2022.03.21	2023.09.24
t_2	96	2022.03.21	2022.06.25
t_3	108	2022.06.25	2022.10.11
t_4	96	2022.10.11	2023.01.15
t_5	96	2023.01.15	2023.04.21
t_6	96	2023.04.21	2023.07.26
t_7	60	2023.07.26	2023.09.24

2.3.3. Processing of input and output data

To process the input and output data in ArcMap version 10.8.1, a raster model was created, incorporating groundwater data, sediment transmissivity, sediment thickness, and ground deformation results obtained from the InSAR method at the neural network's output. In the generated raster model, some pixels representing ground displacement lack subsidence data due to distortions inherent in the InSAR technique. Consequently, these pixels were excluded from the calculations. To ensure full compatibility across the raster models, the pixel dimensions must be consistent. In this study, each raster model pixel was set to dimensions of 206 by 116.

In this study, MATLAB version R2022b was used for coding. The input data, including groundwater level, sediment thickness, and aquifer transmissivity, are represented as a 206x116 matrix. The output data, consisting of subsidence results obtained from SNAPP software, is also represented as a 206x116 matrix for the study area. All input and output parameters are defined as X and T, respectively. The specific input and output parameters corresponding to each time interval are labeled as X1, X2, X3, X4, X5, X6, X7, and T1, T2, T3, T4, T5, T6, T7.

2.3.4. Training of the MLP neural network

To evaluate and predict the performance of the neural network model when new input data is applied, validation data is utilized. If the validation does not meet the required criteria, the learning process is terminated. The validation data is selected from the training dataset (Demuth et al., 2014). In this study, 70% of the dataset is allocated to the training data, 15% to the test data, and 15% to the validation data using a trial-and-error approach. To model the displacements of the Earth's crust over the study period using a multilayer perceptron neural network, a two-layer model is designed. The sigmoid function is used as the activation function, while the Levenberg-Marquardt algorithm is employed as the optimizer. The model consists of four components: an input layer, 100 hidden neurons, an output layer, and an optimization function.

3. Results and discussion

3.1. The Impact of hydraulic and hydrological parameters

To clarify the relationship between the factors influencing subsidence and the vertical displacements of the Earth's crust, a cross-sectional profile (A-B) was drawn. The A-B cross-section is a straight line along which the rate of each parameter can be observed at the points where the profile passes through. As shown in Fig. 5, the greatest subsidence has occurred in the central and western regions, which are primarily used for agricultural and residential purposes. The A-B cross-section spans the Dehgolan Plain aquifer from west to east. To investigate and compare the subsidence rate with groundwater level changes, diagrams illustrating the vertical displacement rate and groundwater level changes were plotted and aligned according to Fig. 5. By comparing the two diagrams of subsidence rate and groundwater level changes, it is evident that maximum subsidence occurs at locations where the most significant decline in groundwater level has taken place. Furthermore, the groundwater level and ground subsidence diagrams exhibit similar trends.

Based on the aquifer transmissivity data and associated maps, a transmissivity profile graph was constructed. The analysis of the aquifer transmissivity map reveals that the highest values of transmissivity are located within the Talvar River region. Additionally, considering the relationship $T=K \cdot b$, where T represents transmissivity, K is hydraulic conductivity, and b is aquifer thickness, it can be inferred that both hydraulic conductivity and aquifer thickness play significant roles in determining aquifer transmissivity. These two parameters are directly related, meaning that changes in either hydraulic conductivity or aquifer thickness lead to corresponding variations in transmissivity.

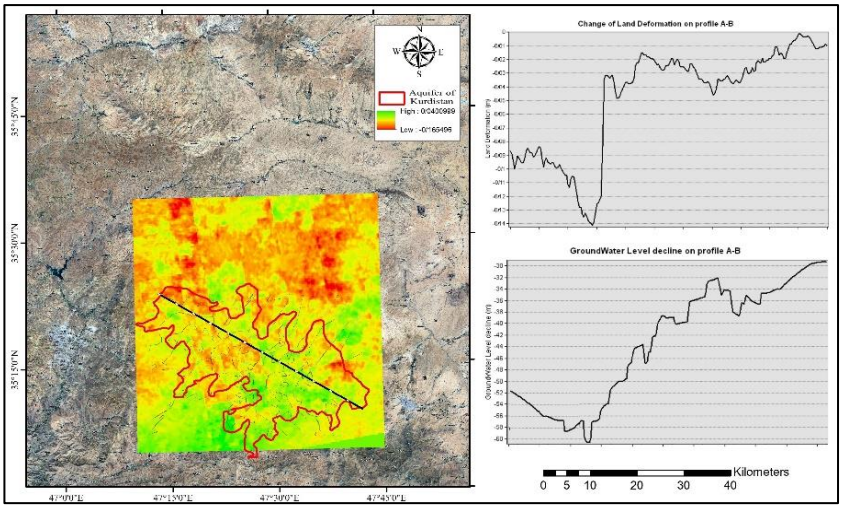

Fig. 5 Subsidence diagram compared to groundwater level decline along the length of the transverse profile A -B

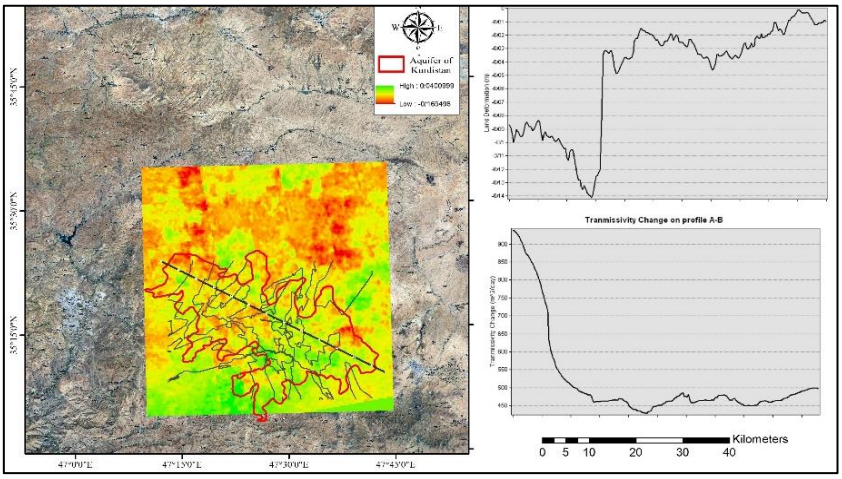

Fig. 6 Subsidence Curve and Aquifer Transmissivity along the A-B Transverse Profile

According to Fig. 6, a comparison between the transmissivity graph and the displacement. Subsidence data in the study area reveals that the progression trend along the profile is not uniform from west to east. Furthermore, areas with higher transmissivity values do not necessarily correspond to lower subsidence rates.

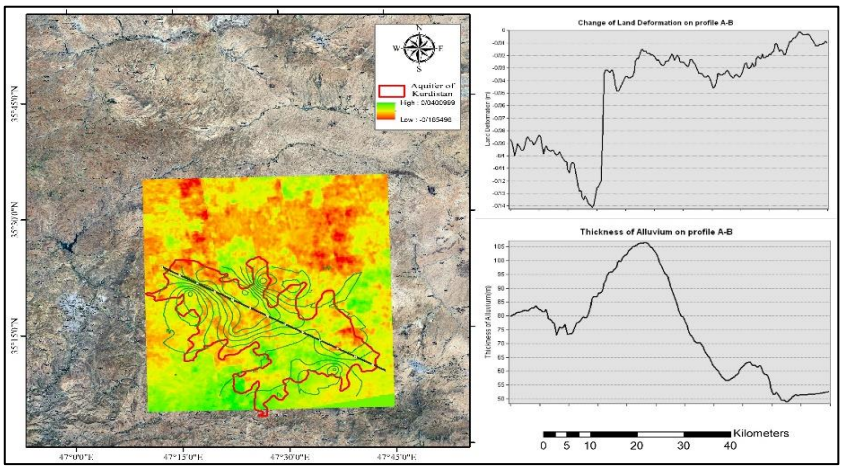

Fig. 7 Comparison of the subsidence diagram with sediment thickness along the length of the A-B transverse profile

Fig. 7 illustrates a comparison between the ground surface displacement diagram and the sediment thickness parameter in the Dehgolan Plain, Kurdistan Province. Both the sediment thickness and subsidence diagrams show an upward trend along the cross-section profile; however, they do not follow identical patterns. This indicates that there is no direct correlation between these two parameters, and an increase in

sediment thickness does not necessarily result in an increase in subsidence.

In general, in alluvial regions, an increase in sediment thickness leads to the loosening of the soil, which contributes to subsidence. However, other factors such as the presence of plant roots, soil substrate, and land use can enhance the soil's relative strength, partially counteracting the effect of sediment thickness on subsidence. Therefore, while sediment thickness is a contributing factor to subsidence, it does not have a direct, one-to-one relationship with the degree of subsidence.

3.2. Multilayer perceptron neural network method

In this research, a multilayer perceptron (MLP) neural network with a backpropagation algorithm was employed to estimate and model land subsidence. Fig. 8 illustrates the relationship between the subsidence values obtained from satellite images using the Interferometric Synthetic Aperture Radar (InSAR) method and the subsidence predicted by the MLP model. The variables T and Y represent the subsidence values derived from InSAR and the predictions made by the MLP model, respectively. As shown in Fig. 8a, the simulation of subsidence is highly accurate, demonstrating a strong correlation between the observed and predicted values. The regression coefficient of 0.87 indicates a very strong relationship between Y and T. However, due to the long time span and the inclusion of both direct and indirect influencing factors as inputs, which increased data complexity, the regression coefficient is slightly lower than 1. In MLP neural networks, a regression value above 0.6 signifies good model performance, with values closer to 1 indicating better accuracy.

Additional information, including the error rate and regression coefficients for the four cases (training, testing, validation, and all data), is presented in Table 2. The average regression value across all cases is 0.875. As shown in Fig. 8b, the error was calculated using the Root Mean Square Error (RMSE), which has a very small average value of 7.041 mm. Furthermore, the error frequency diagram indicates an almost equal distribution of overestimation and underestimation values at all points, with a frequency value of 0.00018.

Table 2 Error values and regression coefficients calculated for the period t_1

Type of Data	RMSE (mm)	MSE (mm)	Regression
Train	6.7943	46.163	0.8847
Test	7.6198	58.062	0.8548
Validation	7.5543	57.067	0.8548
All	7.0416	49.583	0.8755

The spatial distribution of pixels and the simulated subsidence rates in the studied aquifer are presented using a multilayer perceptron (MLP) model, alongside the subsidence rates obtained from satellite images over the entire study period, as shown in Fig. 9. According to the figure, the model's predictions exhibit a reasonable level of accuracy compared to the results derived from the InSAR method. As illustrated in Fig. 9, areas where the subsidence rate is marked as NAN due to missing data, and locations with maximum subsidence (greater than 100 mm), show that the subsidence calculated using InSAR (Fig. 9a) and the subsidence predicted by the MLP model (Fig. 9b) align perfectly. The maximum subsidence rate calculated for the time interval (t_1) using the MLP model is -145.933 mm, while the uplift rate is +12.944 mm.

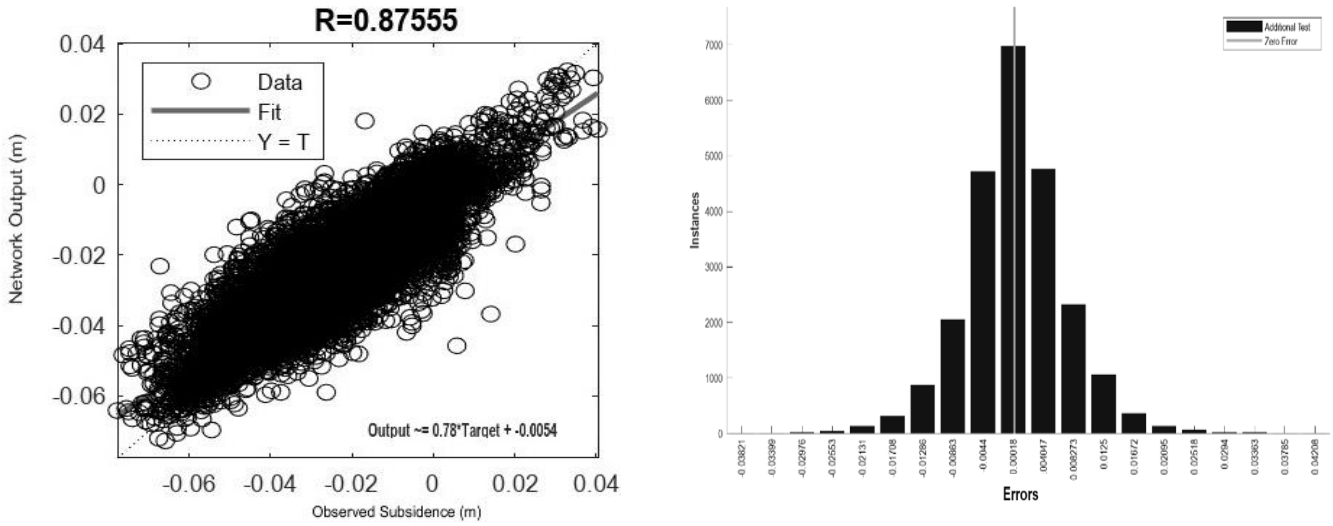

Fig. 8 The results of the predicted model in the time period t_1: a) Regression diagram between the available and predicted data and b) Error frequency diagram of the predicted model

The spatial distribution of pixels and the simulated subsidence rates in the studied aquifer are presented using a multilayer perceptron (MLP) model, alongside the subsidence rates obtained from satellite images over the entire study period, as shown in Fig. 9. According to the figure, the model's predictions exhibit a reasonable level of accuracy compared to the results derived from the InSAR method. As illustrated in Fig. 9, areas where the subsidence rate is marked as NAN due

to missing data, and locations with maximum subsidence (greater than 100 mm), show that the subsidence calculated using InSAR (Fig. 9a) and the subsidence predicted by the MLP model (Fig. 9b) align perfectly. The maximum subsidence rate calculated for the time interval (t_1) using the MLP model is -145.933 mm, while the uplift rate is +12.944 mm.

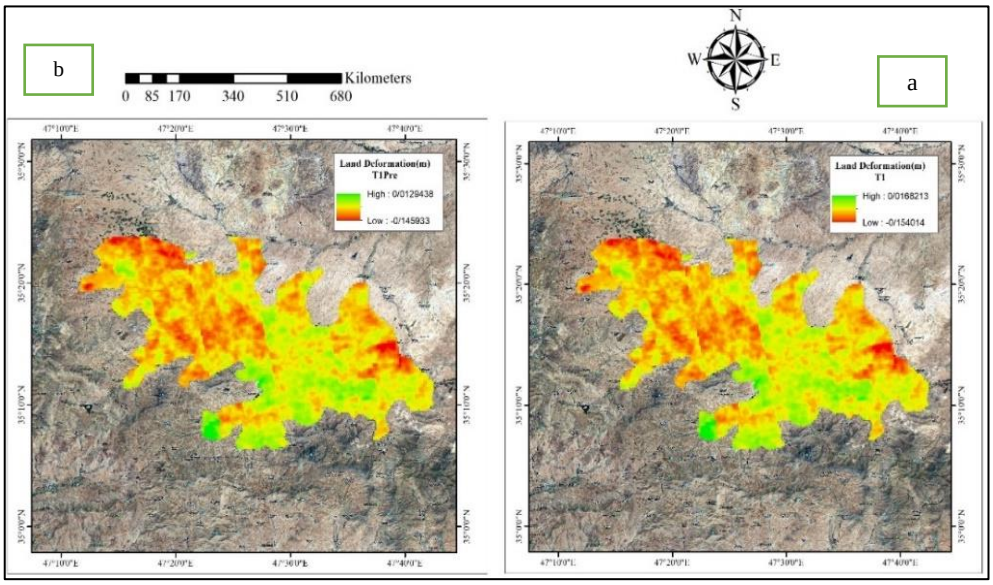

Fig. 9 The geometric location of the subsidence rate estimated in the time interval t_1: a) from the radar interferometric method and b) estimated by the MLP model

The average regression coefficient for the other time periods was 0.92. The results indicate that, except for the time period t_2, the performance of the multilayer perceptron neural network simulation was acceptable and improved from time period (t_1). Due to inherent geometric distortions in radar images during time period t_2, the subsidence results calculated using InSAR in this period exhibit a relative error. However, the trained MLP model was able to detect this error with acceptable accuracy. Consequently, the regression between the results obtained from the InSAR method and the MLP neural network in time period (t_2) is lower than in the other periods, with an estimated value of 0.73. These findings suggest that factors such as the time period, the number of effective parameters, and the complexity of the data—including seasonal changes, geometric distortions, radar image artifacts, construction activities, and especially agricultural activities—affect the amount of vertical ground displacement and reduce the accuracy of the system.

One of the valuable capabilities of neural networks, which is crucial in data science and understanding complex models, is their ability to generalize. In this research, to leverage this capability, the training process was performed using data from the first period of Ordibehesht 1402 to the fourth of Mordad 1402 (t_6). Subsequently, the time period (t_7) was used to simulate and generalize the subsidence model. As shown in Fig. 11-a, the regression coefficient between the subsidence calculated using Sentinel-1 satellite data and the new model for time period t_7 is 0.935. Furthermore, by comparing the estimated subsidence from the MLP model with the subsidence obtained from satellite images (Fig. 10), it is evident that the model performs well in predicting subsidence during time period t_7, with the results being largely consistent.

The satisfactory and reliable performance of the multilayer perceptron neural network model in predicting subsidence over various time intervals can be attributed to several key factors. These include the application of specific filters to each dataset to eliminate noise and outliers, the appropriate allocation of data within the neural network, and the effective training of the model, such as selecting the optimal number of hidden layers and the proportion of data used for training. These steps collectively ensure the development of an optimal model that minimizes errors. Consequently, any alteration in these factors will influence the final results, underscoring the necessity of evaluating the model using validation data to ensure its robustness.

The subsidence results obtained in this study for the study area are highly consistent with those of previous research, such as the study by Ghahroudi Tali et al. (2023). Additionally, studies by Ahmadi and Soudmand Afshar (2020) further support these findings. As demonstrated in this research, there is clear evidence of the direct impact of the groundwater parameter on the variation of subsidence rates, highlighting its significant role in influencing subsidence dynamics. In the study by Edalat et al. (2020), in addition to examining the impact of groundwater level decline on subsidence rate increases using the MLP neural network, the effects of other parameters such as the modulus of elasticity of sediments, sediment thickness, and water transmissivity were also considered. The regression coefficient reported in that study was 0.97, with a mean squared error of 0.0872. These results are estimated to be higher than those obtained in the present study, primarily due to the inclusion of the modulus of elasticity as an effective parameter and differences in model training techniques. Thus, while increasing the number of effective parameters can potentially improve model performance, the results obtained in this study remain reliable and acceptable.

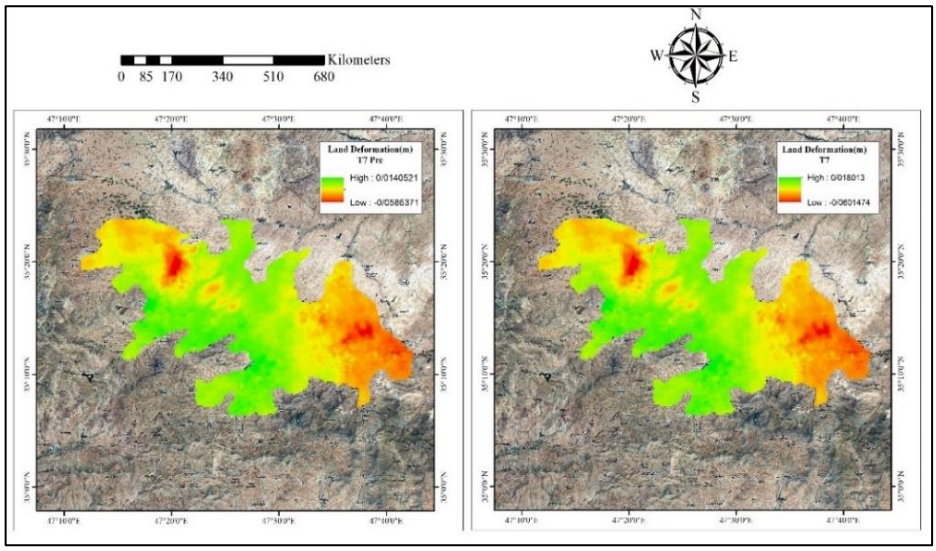

Fig. 10 The results of the geometric location of the subsidence rate of the time period t_7: a) Estimated by the radar interferometric method and b) Predicted by the MLP model

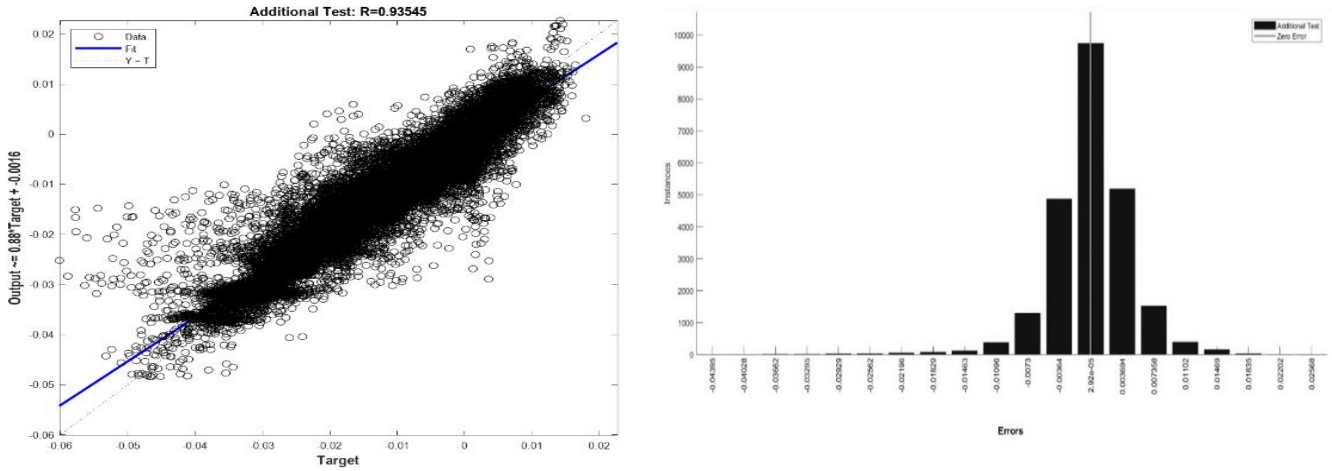

Fig. 11 The results of the predicted model in the time period t7: a) Regression diagram between the available and predicted data and b) Error frequency diagram of the predicted model

4. Conclusion

A multi-layer perceptron (MLP) neural network was employed to assess and monitor land subsidence in the Dehgolan Plain. The key findings of the study are as follows:

1. The maximum subsidence rate calculated using the MLP model was -145.094 mm. When compared to the subsidence rate obtained via the InSAR method, the difference of 8.081 mm is minimal, indicating the satisfactory performance of the model.

2. The MLP neural network calculated an average regression coefficient of 0.8755 for subsidence values across all training, testing, and validation periods (t_1). Additionally, the mean error across all data was 7.041 mm.

3. The results for predicting the subsidence rate during the timeframe (t_7) demonstrate that the model accurately predicts all points, with a mean error of 4.5 mm. Additionally, the model effectively handled NAN points (pixels missing spatial subsidence data) and accurately modeled the maximum subsidence rate.

4. The flexibility and generalization capabilities of the neural network make it a powerful and cost-effective tool for addressing complex problems in the field of water resources and destructive phenomena, such as subsidence, by defining an appropriate network architecture.

Limitations of this study include the absence of global positioning stations for continuous monitoring of subsidence in vulnerable and affected areas, a lack of verified data for accurate subsidence assessment, and the large volume of image and radar data required for long-term InSAR analysis.

Research Statement

Data Availability

The datasets generated during and.or analyzed during the current study are available from the corresponding author on reasonable request.

Conflicts of interest

The authors of this paper declared no conflict of interest regarding the authorship or publication of this article.

Author contribution

S. M. Hosseini: Modeling and Results Analysis; M. Isari: Results Analysis and Research Management; J. Bahrami:

Research Management; S. Karimi: Data Collection and F. Faghihi: Data Collection.

References

Abrahart, R., & White, S. (2001). Modelling sediment transfer in Malawi: comparing backpropagation neural network solutions against a multiple linear regression benchmark using small data sets. Phys. Chem. Earth, Part B: *Hydrol., Ocean. Atm.*, *26*(1), 19-24. DOI: 10.1016/S1464-1909(01)85008-5

Ahmadi, S., & Soudmand Afshar, R. (2020). Monitoring of land subsidence in Qorveh and Chahardoli Plains of Hamadan and Kurdistan Provinces using PS-InSAR Technique. *Environ. Water Eng.*, *6*(3), 219-233. DOI: 10.22034/jewe.2020.236939.1375

Ali, M. Z., Chu, H.-J., & Burbey, T. J. (2020). Mapping and predicting subsidence from spatio-temporal regression models of groundwater-drawdown and subsidence observations. *Hydrogeol. J.*, *28*(8). DOI: 10.1007/s10040-020-02211-0

Asghari Moghaddam, A., Nouri Sangarab, S., & Kadkhodaie Ilkhchi, A. (2023). Assessing groundwater vulnerability potential using modified DRASTIC in Ajabshir Plain, NW of Iran. *Environ. Monit. Assess.*, *195*(4), 497. DOI: 10.1007/s10661-023-10992-6

Anonymous. (2018). Report on the extension and development of the prohibition level of the study area of Qorveh-Dehgolan .*Kurdestan Water and Wastewater Company*.

Banerjee, P., Singh, V., Chatttopadhyay ,K., Chandra, P., & Singh, B. (2011). Artificial neural network model as a potential alternative for groundwater salinity forecasting. *J. Hydrol*, *398*(3-4), 212-220. DOI: 10.1016/j.jhydrol.2010.12.016

Demuth, H. B., Beale, M. H., De Jess, O., & Hagan, M. T. (2014). *Neural network design*. Martin Hagan.

Edalat, A., Khodaparast, M., & Rajabi, A. M. (2020). Detecting land subsidence due to groundwater withdrawal in Aliabad Plain, Iran, using ESA sentinel-1 satellite data. *Nat. Resour. Res.*, *29*, 1935-1950. DOI: 10.1007.s11053-019-09546-w

Ghahroudi Tali, M., Khodamoradi, F., & Ali Nouri, K. (2023). Effects of groundwater decrease on the of land subsidence in Dehgolan plain, Kurdistan province. *Environ. Manage. Haz.*, *10*(1), 57-70. DOI: 10.22059/JHSCI.2023.359130.777

Ku, C.-Y., & Liu, C.-Y. (2023). Modeling of land subsidence using GIS-based artificial neural network in Yunlin County, Taiwan. *Sci. Report.*, *13*(1), 4090. DOI: 10.1038/s41598-023-31390-5

Hosseinzadeh, E., Anamaghi, S., Behboudian, M., & Kalantari, Z. (2024). Evaluating Machine Learning-Based Approaches in Land Subsidence Susceptibility Mapping. *Land*, *13*(3), 322. DOI: 10.3390/land13030322

Radman, A., & Akhoondzadeh, M. (2022). Monitoring and modeling of Urmia Lake area variations using artificial neural network. *J. Environ. Stud.*, *46*(2), 295-317. DOI: 10.22059/JES.2021.304189.1008026.

Ranjgar, B., Razavi-Termeh, S. V., Foroughnia, F., Sadeghi-Niaraki, A., & Perissin, D. (2021). Land subsidence susceptibility mapping using persistent scatterer SAR interferometry technique and optimized hybrid machine learning algorithms. *Remote Sens.*, *13*(7), 1326. DOI: 10.3390/rs13071326

Shimosato, K., & Ukita, N. (2021). Multi-modal data fusion for land-subsidence image improvement in PSInSAR analysis. *IEEE Access*, *9*, 141970-141980. DOI: 10.1109/ACCESS.2021.3120133

Wang, Z ,.Li, L., Yu, Y., Wang, J., Li, Z., & Liu, W. (2021). A novel phase unwrapping method used for monitoring the land subsidence in coal mining area based on U-Net convolutional neural network. *Front. Earth Sci.*, *9*, 761653. DOI: 10.3389/feart.2021.761653

Zhang, B., Xu, C., Dai, X., & Xiong, X. (2024). Research on mining land subsidence by intelligent hybrid model based on gradient boosting with categorical features support algorithm. *J. Environ. Manage.*, *354*, 120309. DOI: 10.1016/j.jenvman.2024.120309

Zhao, R., Arabameri, A., & Santosh, M. (2024). Land subsidence susceptibility mapping: a new approach to improve decision stump classification (DSC) performance and combine it with four machine learning algorithms. *Environ. Sci. Pollut. Res.*, *31*(10), 15443-15466. DOI: 10.1007/s11356-024-32075-w

Zhou, D., Zuo, X., & Zhao, Z. (2022). Constructing a large-scale urban land subsidence prediction method based on neural network algorithm from the perspective of multiple factors. *Remote Sens.*, *14*(8), 1803. DOI: 10.3390/rs14081803

Zhu, X., Zhu, W., Guo, L., Ke, Y., Li, X., Zhu, L., Sun, Y., Liu, Y ,.Chen, B., & Tian, J. (2023). Study on Land Subsidence Simulation Based on a Back-Propagation Neural Network Combined with the Sparrow Search Algorithm. *Remote Sens.*, *15*(12), 2978. DOI: 10.3390/rs15122978